J. Fluid Mech. (1990), *vol.* 218, *pp.* 1–17
Printed in Great Britain

Sand ripples under sea waves
Part 1. Ripple formation

By P. BLONDEAUX
Istituto di Idraulica, Università di Genova, Via Montallegro, 1, 16145 Genova, Italy

(Received 1 December 1988 and in revised form 14 June 1989)

In the present paper we formulate a predictive theory of the formation of sand ripples under sea waves. The theory is based on a linear stability analysis of a flat sandy bottom subject to a viscous oscillatory flow. The conditions for decay or amplification of a bottom perturbation are determined along with the wavelength of the most unstable component as a function of the Reynolds number of the flow and of the Froude and Reynolds numbers of the sediments. A comparison between theoretical findings and experimental data supports the validity of the present theory. An analytical solution for viscous oscillatory flow over a small-amplitude wavy bottom is determined for arbitrary values of the ratio r between the amplitude of fluid displacement and the wavelength of bottom waviness. Previous works by Lyne (1971) and Sleath (1976), who considered small or large values of r, are thus extended.

1. Introduction

Sand ripples are bedforms known to occur at the bottom of sea waves in shallow waters. Their practical interest arises in connection with the study of sand transport and wave damping in nearshore regions.

The mechanics of ripple formation is qualitatively understood. Indeed it is known (Sleath 1984) that a small spatially periodic perturbation of the sea bottom under wave action produces steady streaming which consists of recirculating cells, the form, intensity and direction of which depend on the characteristics of the wave and of the perturbation. Because the sediment is driven by the fluid, if the steady drift in the vicinity of the bed is directed from the troughs towards the crests of the perturbation and is strong enough, the latter grows and a pattern of regular or irregular sandy waves appears.

On the basis of experiments, Bagnold (1946) distinguished 'rolling-grain ripples' from 'vortex ripples'. He observed that rolling-grain ripples, characterized by the absence of separation behind the crests, are the first to appear on an initially plane bed subject to wave action. Increasing the amplitude of velocity oscillations, flow separates and vortex ripples develop. Rolling-grain ripples have also been observed by Manohar (1955), Horikawa & Watanabe (1968) and Sleath (1976) among others. Recent experiments by Blondeaux, Sleath & Vittori (1988) seem to indicate that a range of the parameters exists within which rolling-grain ripples reach an equilibrium configuration. Other authors have performed experiments in which stable sandy non-separated bottom configurations were not observed, which led to questioning the actual existence of rolling-grain ripples. Notwithstanding this, the importance of investigating the conditions for the development of a small non-separated bottom perturbation by means of a stability analysis stems from the fact that in the first

stage of growth the amplitude of any kind of ripple is so small that vortex formation is inhibited.

Recently Lyne (1971), Uda & Hino (1975), Sleath (1976), Kaneko & Honji (1979), Kaneko (1981) contributed to the explanation of rolling-grain ripple formation by studying the oscillatory viscous flow over a fixed wavy wall with wavelength l^* and amplitude $2\epsilon^*$ under the assumption of small values of ϵ^*/l^* and small or large values of the ratio r between the amplitude of fluid displacement and l^*. In order to determine the conditions of incipient ripple formation, sediment flow rate was then related to fluid flow on the basis of physical arguments. As pointed out by Sleath (1984), the difficulty with the two solutions for small or large values of r is that ripples usually form for values of r of order one.

In the present work we formulate a predictive theory of ripple formation based on a linear stability analysis of a flat sandy bottom subject to a water wave. An analytical solution for the viscous oscillatory flow over a wavy bottom is determined for arbitrary values of r. Previous works on the subject are thus extended in a more significant range of the relevant parameters. A sediment flow rate formula is proposed which is based on physical arguments and on the experimental data of Grass & Ayoub (1982) and Sleath (1978).

The conditions for the decay or the amplification of a sinusoidal perturbation of the bottom are determined and the wavelength of the most unstable disturbance is obtained as a function of three parameters: the Reynolds number of the Stokes layer and the Froude and Reynolds numbers of the sediment.

The present linear analysis is then extended in a companion paper (Vittori & Blondeaux 1990) where nonlinear effects are taken into account. In the latter contribution the time development of an initial small perturbation of the bottom is followed till a finite amplitude is reached. It is found that for some values of the parameters the only possible stable bottom configuration is such that flow separates behind the crests and vortices are generated. This allows the prediction of whether rolling-grain ripples or vortex ripples will develop, depending on wave and sediment characteristics.

In the next section we formulate the problem. In §3 an analytical solution for the oscillatory viscous flow over a wavy bottom is determined for arbitrary values of r. In the following section the time development of the bottom is described. Finally in §5 the results of the linear stability analysis are presented along with some conclusions.

2. Formulation of the problem

Let us consider a two-dimensional gravity wave of small height H^*, length L^* and period T^* in shallow water of depth h^* propagating over an initially flat cohesionless bottom formed by sediment of uniform size d^*, density ρ_s and porosity n. Let us respectively denote by ρ and ν the density and kinematic viscosity of water.

It is well established that the flow can be modelled as irrotational except within the unsteady boundary layer adjacent to the bottom. Since we are interested in the interaction between fluid and sediment, we focus our attention on the latter layer and use linear wave theory to describe the motion outside this region. We assume the characteristic thickness of the bottom boundary layer δ^* to be much smaller than both the water depth and the length of the gravity wave. Flow in the bottom boundary layer can then be considered as caused by fluid oscillations which are only parametrically dependent on the longitudinal coordinate. We define a Cartesian orthogonal coordinate system (x^*, y^*) with the x^* axis lying on the bottom and

parallel to the direction of wave propagation, the y^* axis directed upward. The above assumptions allow us to assume the following form for the velocity vector (u^*, v^*) outside the bottom layer:

$$(u^*, v^*) = (-\tfrac{1}{2}U_0^* \, \mathrm{e}^{\mathrm{i}\omega^* t^*} + \text{c.c.}, 0) \tag{1}$$

where t^* is time, $\omega^* = 2\pi/T^*$ angular frequency, U_0^* the amplitude of the irrotational velocity oscillations evaluated at the bottom and c.c. denotes the complex conjugate of a complex number.

If the bottom is flat and d^* is much smaller than the characteristic thickness of the bottom boundary layer δ^*, the fluid motion is described by the well known Stokes' (1851) solution and the sediment moves to and fro. If the flow is laminar δ^* can be assumed to be equal to $(2\nu/\omega^*)^{\frac{1}{2}}$: this occurs provided the Reynolds number characteristic of the bottom boundary layer ($R_\delta = U_0^* \delta^*/\nu$) does not exceed the value for which flow disturbances grow and turbulence develops (Merkly & Thomann 1975; Hino, Sawamoto & Takasu 1976; Tromans 1976; Blondeaux & Seminara 1979; Blondeaux 1987).

Let us consider a bottom perturbation in the form

$$y^* = \eta^*(x^*, t^*) = \epsilon^* C_1(t^*) \, \mathrm{e}^{\mathrm{i}\alpha^* x^*} + \text{c.c.} \tag{2}$$

with wavenumber α^* and 'small' (strictly infinitesimal) amplitude $2\epsilon^* C_1(t^*)$.

The study of flow and bottom development in the new configuration is posed by the vorticity equation, the flow and sediment continuity equations and boundary conditions which force the matching of the flow with the irrotational motion outside the bottom boundary layer and the no-slip condition at $y^* = \eta^*$.

Let us define the following dimensionless variables:

$$\left.\begin{aligned} (x, y) &= \frac{(x^*, y^*)}{\delta^*}, \quad t = t^* \omega^*, \quad \epsilon = \frac{\epsilon^*}{\delta^*}, \quad \alpha = \alpha^* \delta^*, \\ \eta &= \frac{\eta^*}{\delta^*}, \quad \psi = \frac{\psi^*}{U_0^* \, \delta^*}, \quad q = \frac{q^*}{[((\rho_s/\rho) - 1) \, g d^{*3}]^{\frac{1}{2}}} \end{aligned}\right\} \tag{3}$$

where g is gravity, ψ^* is the stream function (ψ^* is such that $u^* = \partial\psi^*/\partial y^*$ and $v^* = -\partial\psi^*/\partial x^*$) and q^* is sediment flow rate. The governing differential problem then reads (Sleath 1976)

$$\frac{2}{R_\delta} \frac{\partial}{\partial t}(\nabla^2\psi) + \frac{\partial\psi}{\partial y}\frac{\partial}{\partial x}(\nabla^2\psi) - \frac{\partial\psi}{\partial x}\frac{\partial}{\partial y}(\nabla^2\psi) = \frac{1}{R_\delta}(\nabla^4\psi), \tag{4}$$

$$\frac{\partial q}{\partial x} = -\frac{2F_d}{R_d}(1-n)\frac{\partial\eta}{\partial t}, \tag{5}$$

$$\frac{\partial\psi}{\partial y} \to -\tfrac{1}{2}\mathrm{e}^{\mathrm{i}t} + \text{c.c.}, \quad \frac{\partial\psi}{\partial x} \to 0 \quad \text{for} \quad y \to \infty, \tag{6}$$

$$\frac{\partial\psi}{\partial y} = 0, \quad \frac{\partial\psi}{\partial x} = 0 \quad \text{for} \quad y = \eta, \tag{7}$$

where the parameters particle Reynolds number R_d, particle Froude number F_d and the ratio between sediment and fluid densities s are defined in the form

$$F_d = \frac{U_0^*}{[((\rho_s/\rho) - 1) \, g d^*]^{\frac{1}{2}}}, \quad R_d = \frac{U_0^* d^*}{\nu}, \quad s = \frac{\rho_s}{\rho}. \tag{8}$$

In order to close the above formulation, we need a relationship between sediment flow rate q^* and flow properties. A relationship can be simply obtained by relating q^* to the agitating forces which act on sediment grains. The latter move subject to the drag force and to the gravity component along the bed profile, other forces being negligible. Indeed for values of U_0^*, T^* and d^* characteristic of sediments at the bottom of gravity waves, the Keulegan–Carpenter number of the phenomenon is large and the forces acting on the particle related to flow acceleration can be neglected. Following an approach which has widely been used in research on steady sediment transport (Engelund 1974), sediment flow rate can be assumed to be proportional to some power b of the agitating forces. If we assume that the drag force is proportional to $\mu V^* d^*$ and the gravity component along the bed profile to $(\rho_s-\rho) g d^{*3} (\partial\eta^*/\partial x^*)$ (V^* being fluid velocity parallel to the bottom profile evaluated at $y^* = \frac{1}{2} d^*$ and μ the dynamic viscosity of the fluid), in a dimensionless form we may write

$$q = a \left| \frac{2}{R_d} V - \frac{\beta}{F_d^2} \frac{\partial \eta}{\partial x} \right|^b \operatorname{sgn}\left(\frac{2}{R_d} V - \frac{\beta}{F_d^2} \frac{\partial \eta}{\partial x} \right). \tag{9}$$

The constant β in (9) was introduced by Fredsøe (1974) in a different context. The values of a and b can be estimated in the relevant range of the parameters (i.e. for $R_d < R_\delta$) by requiring that relationship (9) should match the empirical law proposed by Grass & Ayoub (1982).

It is found that a is a function of s, R_d and F_d ($a = 1.23\ (s - 1/s)\ F_d^{6.72} R_d^{1.83}$) and b is equal to 4.28. Moreover the value 0.15 has been employed for β, following Fredsøe (1974). Here a is related to the amount of sediment moved by the flow and b to its temporal development.

The results described below and those of Vittori & Blondeaux (1990) are not affected by the value of a, which consequently does not play any role in the present analysis. On the other hand, variations of b imply significant modifications of the results. The agreement between the time development of the sediment flow rate determined by means of (9) with b equal to 4.28 and that found experimentally by Sleath (1978) supports the proposed formula.

It is worth pointing out that using a sediment transport model which lacks a threshold condition for sediment motion is equivalent to ignoring the portion of the cycle when the instantaneous conditions lie below the threshold conditions for sediment motion. This approximation is quite advantageous from an analytical point of view because it avoids the need to model the discontinuous behaviour of sediment transport and is justified whenever the actual values of the parameters are well beyond the critical values corresponding to the threshold conditions for sediment motion. Indeed in this situation the portion of the cycle when sediment grains do not move is negligible. When ripples appear at the bottom of gravity waves sediment motion is usually well established.

The above derivation of (9), though simple and possibly rough, appears to contain the main physical ingredients controlling the process of transport. It will be shown that when applied to the process of ripple formation it performs fairly well.

We then consider bottom perturbations of small amplitude and assume $\epsilon \ll 1$. The solution of the problem (4), (7) is thus developed in power series of ϵ in the form

$$\psi = \psi_0(y,t) + \epsilon C_1(t)\, \Phi_1(y,t)\, e^{i\alpha x} + \text{c.c.} + O(\epsilon)^2, \tag{10}$$

$$q = q_0(t) + \epsilon C_1(t)\, q_1(t)\, e^{i\alpha x} + \text{c.c.} + O(\epsilon^2). \tag{11}$$

By substituting from (10), (11) into (4)–(7) and equating like powers of ϵ we find

$O(\epsilon^0)$

$$\frac{2}{R_\delta}\frac{\partial}{\partial t}\left(\frac{\partial^2\psi_0}{\partial y^2}\right)=\frac{1}{R_\delta}\left(\frac{\partial^4\psi_0}{\partial y^4}\right), \tag{12}$$

$$\left.\begin{aligned}&\frac{\partial\psi_0}{\partial y}\to-\tfrac{1}{2}e^{it}+\text{c.c.}, && y\to\infty\\&\frac{\partial\psi_0}{\partial y}=0, && y=0,\end{aligned}\right\} \tag{13}$$

$$q_0(t)=a\left|\frac{2}{R_d}\frac{\partial\psi_0}{\partial y}\right|^b\operatorname{sgn}\left(\frac{2}{R_d}\frac{\partial\psi_0}{\partial y}\right),\quad y=\frac{R_d}{2R_\delta} \tag{14}$$

$O(\epsilon^1)$

$$\frac{2}{R_\delta}\frac{\partial}{\partial t}\left(\frac{\partial^2\Phi_1}{\partial y^2}-\alpha^2\Phi_1\right)+i\alpha\left[\frac{\partial\psi_0}{\partial y}\left(\frac{\partial^2\Phi_1}{\partial y^2}-\alpha^2\Phi_1\right)-\frac{\partial^3\psi_0}{\partial y^3}\Phi_1\right]$$
$$=\frac{1}{R_\delta}\left[\frac{\partial^4\Phi_1}{\partial y^4}-2\alpha^2\frac{\partial^2\Phi_1}{\partial y^2}+\alpha^4\Phi_1\right], \tag{15}$$

$$\left.\begin{aligned}&\frac{\partial\Phi_1}{\partial y}\to0, && \Phi_1\to0, && y\to\infty\\&\frac{\partial\Phi_1}{\partial y}=-\frac{\partial^2\psi_0}{\partial y^2}, && \Phi_1=0, && y=0,\end{aligned}\right\} \tag{16}$$

$$-\frac{2F_d}{R_d}(1-n)\frac{dC_1(t)}{dt}=i\alpha q_1(t)C_1(t), \tag{17}$$

$$q_1(t)=ab\left|\frac{2}{R_d}\frac{\partial\psi_0}{\partial y}\right|^{b-1}\frac{2}{R_d}\left[\frac{\partial^2\psi_0}{\partial y^2}+\frac{\partial\Phi_1}{\partial y}-\frac{i\alpha\beta R_d}{2F_d^2}\right],\quad y=\frac{R_d}{2R_\delta}. \tag{18}$$

We point out that at order ϵ, the term proportional to the time derivative of $C_1(t)$ in the vorticity equation has been neglected. From a physical point of view, this corresponds to neglecting the influence of the variation of bottom elevation on fluid motion. From a mathematical point of view, this assumption is justified by the small value usually attained by the dimensionless parameter

$$Q=\frac{aR_d^{1-b}}{(1-n)\,2F_d}\sim\frac{dC_1(t)}{dt}\Big/C_1(t).$$

3. Flow solution

In order to determine the stream function ψ and thus the flow field, it is convenient to adopt a coordinate system $(\tilde{x},\tilde{y})$ which moves with the fluid far from the bottom. Let us then write,

$$\tilde{x}=x+\tfrac{1}{4}R_\delta\int_0^t(e^{it}+\text{c.c.})\,dt,\quad \tilde{y}=y. \tag{19}$$

The transformation (19) reduces the problem to the equivalent problem of the flow induced by the harmonic oscillation of a wavy wall in a fluid otherwise at rest. The wall motion is described by the equation,

$$\tilde{y}_{\text{wall}} = \epsilon \exp\left[-\tfrac{1}{4}\mathrm{i}\alpha R_\delta \int_0^t (\mathrm{e}^{\mathrm{i}t} + \text{c.c.})\,\mathrm{d}t\right] \mathrm{e}^{\mathrm{i}\alpha\tilde{x}} + \text{c.c.} = \epsilon P(t)\,\mathrm{e}^{\mathrm{i}\alpha\tilde{x}} + \text{c.c.}, \tag{20}$$

The stream function $\tilde{\psi}$ in the new reference frame is related to ψ by

$$\tilde{\psi} = \psi + \tfrac{1}{2}(\mathrm{e}^{\mathrm{i}t} + \text{c.c.})\,\tilde{y}, \tag{21}$$

whence

$$\tilde{\psi}_0 = \psi_0 + \tfrac{1}{2}(\mathrm{e}^{\mathrm{i}t} + \text{c.c.})\,\tilde{y}, \quad \tilde{\Phi}_1 = \Phi_1 P(t), \tag{22a, b}$$

where

$$\tilde{\psi} = \tilde{\psi}_0 + \epsilon(\tilde{\Phi}_1\,\mathrm{e}^{\mathrm{i}\alpha\tilde{x}} + \text{c.c.}). \tag{23}$$

By substituting from (19)–(23) into (12)–(16) we find

$O(\epsilon^0)$

$$\tilde{\psi}_0 = \left[C - \frac{1}{2(1+i)}\mathrm{e}^{-(1+\mathrm{i})\tilde{y}}\right]\mathrm{e}^{\mathrm{i}t} + \text{c.c.} = F_0(\tilde{y})\,\mathrm{e}^{\mathrm{i}t} + \text{c.c.} \tag{24}$$

$O(\epsilon^1)$

$$\frac{2}{R_\delta}\frac{\partial}{\partial t}(\mathrm{N}^2\tilde{\Phi}_1) + \mathrm{i}\alpha\left[\frac{\partial\tilde{\psi}_0}{\partial\tilde{y}}\mathrm{N}^2\tilde{\Phi}_1 - \frac{\partial^3\tilde{\psi}_0}{\partial\tilde{y}^3}\tilde{\Phi}_1\right] = \frac{1}{R_\delta}\mathrm{N}^4\tilde{\Phi}_1, \tag{25}$$

$$\left.\begin{aligned} &\frac{\partial\tilde{\Phi}_1}{\partial\tilde{y}} = -\frac{\partial^2\tilde{\psi}_0}{\partial\tilde{y}^2}P(t), \quad \tilde{\Phi}_1 = 0, \quad \tilde{y} = 0, \\ &\frac{\partial\tilde{\Phi}_1}{\partial\tilde{y}} \to 0, \qquad\qquad\quad \tilde{\Phi}_1 \to 0, \quad \tilde{y} \to \infty, \end{aligned}\right\} \tag{26}$$

where $\mathrm{N}^2 \equiv (\partial^2/\partial\tilde{y}^2 - \alpha^2)$. The solution of equation (25) and boundary conditions (26) can be determined by means of a procedure similar to that used by Seminara & Hall (1976) in a different context.

Let us develop the unknown function $\tilde{\Phi}_1$ in a Fourier series

$$\tilde{\Phi}_1 = \sum_{m=-\infty}^{+\infty} G_m(\tilde{y})\,\mathrm{e}^{\mathrm{i}mt}. \tag{27}$$

By substituting from (27) into the partial differential problem (25), (26) we obtain an infinite set of ordinary differential equations for the coefficients $G_m(\tilde{y})$ $(m = -\infty, \infty)$. An argument similar to that used by Seminara & Hall (1976) then leads to the following structure for the functions G_m:

$$\begin{aligned} G_m(\tilde{y}) = \sum_{n=-\infty}^{+\infty} \Bigg\{ & a_n \sum_{j=0}^{\infty} \lambda_{nmj} \exp\left[-[\alpha + (m-n)\,\mathrm{i} + j)]\,\tilde{y}\right] \\ & + (1-\delta_{n0})\,b_n \sum_{j=0}^{\infty} \vartheta_{nmj} \exp\left[-[\sigma_n + (m-n)\,\mathrm{i} + j]\,\tilde{y}\right] \Bigg\} \\ & + b_0 \sum_{j=0}^{\infty} \{\beta_{mj} \exp\left[-[\alpha + m\mathrm{i} + j)]\,\tilde{y}\right] + \gamma_{mj}\,\tilde{y} \exp\left[-[\alpha + m\mathrm{i} + j]\,\tilde{y}\right]\}, \end{aligned} \tag{28}$$

where $\sigma_n = (\alpha^2 + 2n\mathrm{i})^{\frac{1}{2}}$.

By substituting from (27), (28) into (25) the constants λ_{nmj}, ϑ_{nmj}, β_{mj}, γ_{mj} are found to be given by the following recurrence relationships:

$$\begin{aligned}\lambda_{n,m,j} = {} & \tfrac{1}{2}\mathrm{i}\alpha R_\delta\{\lambda_{n,m-1,j-1}[(\alpha+(m-1-n)\,\mathrm{i}+j-1)^2-\alpha^2-2\mathrm{i}] \\ & +\lambda_{n,m+1,j-1}[(\alpha+(m+1-n)\,\mathrm{i}+j-1)^2-\alpha^2-2\mathrm{i}]\} \\ & \times\{[(\alpha+(m-n)\,\mathrm{i}+j)^2-\alpha^2][(\alpha+(m-n)\,\mathrm{i}+j)^2-\alpha^2-2\mathrm{i}m]\}^{-1}. \qquad (29)\end{aligned}$$

Similar expressions hold for $\vartheta_{nmj}, \beta_{mj}, \gamma_{mj}$.

Finally a_n and b_n are determined by imposing the boundary conditions at $\tilde{y}=0$. This leads to a linear system of algebraic equations for the unknowns a_n and b_n. By truncating at the Mth term the expansion (27) in such a way that the contribution of the harmonics $M+1$ and $-M-1$ to the solution is negligible, the latter system becomes

$$\left.\begin{aligned}&\sum_{n=-M}^{+M} a_n A_{mn}+b_n B_{mn}=0,\\ &\sum_{n=-M}^{+M} a_n C_{mn}+b_n D_{mn}=\tfrac{1}{2}(1+\mathrm{i})\,p_{m-1}+\tfrac{1}{2}(1-\mathrm{i})\,p_{m+1},\end{aligned}\right\} -M<m<+M, \qquad (30)$$

where

$$P(t)=\sum_{m=-M}^{+M} p_m\,\mathrm{e}^{\mathrm{i}mt} \qquad (31)$$

and

$$\left.\begin{aligned}&A_{mn}=\sum_{j=0}^{M}\lambda_{nmj};\\ &B_{mn}=\sum_{j=0}^{M}\vartheta_{nmj}\quad\text{for}\quad(n\neq 0);\quad B_{m0}=\sum_{j=0}^{M}\beta_{mj};\\ &C_{mn}=\sum_{j=0}^{M}-[\alpha+(m-n)\,\mathrm{i}+j]\,\lambda_{nmj};\\ &D_{mn}=\sum_{j=0}^{M}-[\sigma_n+(m-n)\,\mathrm{i}+j]\,\vartheta_{nmj}\quad\text{for}\quad(n\neq 0);\\ &D_{m0}=\sum_{j=0}^{M}-[\alpha+m\mathrm{i}+j]\,\beta_{mj}+\gamma_{mj}.\end{aligned}\right\} \qquad (32)$$

The value of M depends on the parameters of the problem and ranges between few units for small values of αR_δ up to 25 for the largest value of αR_δ investigated in the present paper.

The problem is then reduced to the solution of the linear algebraic system (30). Results obtained using the above procedure will be described in §5.

4. Bottom development

Once the stream function is known, one can easily solve for the bottom development substituting from (22*a*, *b*) and (18) into (17). We find

$$\begin{aligned}\frac{\mathrm{d}C_1}{\mathrm{d}t} &= -\mathrm{i}\alpha Qb2\left|2\frac{\partial\psi_0}{\partial y}\right|^{b-1}\left[\frac{\partial^2\psi_0}{\partial y^2}+\frac{\partial\Phi_1}{\partial y}-\frac{\mathrm{i}\alpha\beta R_d}{2F_d^2}\right]C_1(t)\\ &= \mathscr{A}(t,\alpha,R_\delta,R_d,F_d)\,C_1(t), \qquad (33)\end{aligned}$$

whence

$$C_1(t)=C_0\exp\left[\int_{t_0}^{t}\mathscr{A}(\tau,\alpha,R_\delta,R_d,F_d)\,\mathrm{d}\tau\right]. \qquad (34)$$

Four contributions to $C_1(t)$ can be identified. The first two contributions are related to the real ($\tilde{\mathscr{A}}_r$) and imaginary ($\tilde{\mathscr{A}}_i$) parts of the time average of the function $\mathscr{A}(t)$

$$\tilde{\mathscr{A}}_r + i\tilde{\mathscr{A}}_i = \frac{1}{2\pi}\int_0^{2\pi} \mathscr{A}(t, \alpha, R_\delta, R_d, F_d)\, dt. \tag{35}$$

The real part $\tilde{\mathscr{A}}_r$ controls the amplification of the bottom perturbation, while the imaginary part $\tilde{\mathscr{A}}_i$ is its wave speed. The latter must vanish for the symmetry of the problem. The third and fourth contributions are related to the oscillating parts of $\mathscr{A}(t)$

$$\int_{t_0}^{t} [\mathscr{A}(\tau, \alpha, R_\delta, R_d, F_d) - (\tilde{\mathscr{A}}_r + i\tilde{\mathscr{A}}_i)]\, d\tau. \tag{36}$$

They describe the time variation of the perturbation profile during a wave cycle. More precisely the real part describes oscillations of the amplitude of bottom perturbation while the imaginary part controls the small longitudinal oscillations of the ripple profile around its average position.

The growth of perturbations and consequently ripple formation is thus controlled by the sign of $\tilde{\mathscr{A}}_r$, the value of which is negative or positive depending on the values attained by the flow and sediment parameters $\alpha, R_\delta, R_d, F_d$ as described in the following section.

5. Results and discussion

As discussed above the steady streaming associated with secondary flow induced by bottom perturbations plays a crucial role in controlling ripple growth. Let us then first discuss our solution for the flow field.

For low values of R_δ and large values of α such that αR_δ is smaller than one, the steady streaming consists of two recirculating cells (see figure 1) and the flow near the bottom is directed from the troughs towards the crests of the perturbation. Decreasing α below a threshold value $\tilde{\alpha}$, the flow pattern exhibits the presence of four cells (see figure 2). In this case, even though near the wall the flow is directed from the troughs towards the crests, a region close to the bottom exists where the flow direction reverses. This agrees well with results of previous authors (Lyne 1971; Sleath 1976; Kaneko & Honji 1979) who studied the oscillatory flow over a wavy wall in the limit of αR_δ vanishing. Quantitative comparison with the latter authors is not shown in figures 1, 2 since the patterns of steady streaming are practically identical. On increasing the value of R_δ in such a way that the ratio between the amplitude of fluid displacement and the wavelength of the bottom perturbation be of order one a similar behaviour is found (notice that ripples in the field are characterized by values of αR_δ of order one). However, as R_δ increases, the value of $\tilde{\alpha}$ for which four cells appears first increases and then monotonically decreases.

At present it is impossible to compare the present results with those of Lyne (1971) in the limit of $r \to \infty$, since the present method becomes exceedingly expensive when r is larger than 10. For $r = 10$ the results obtained show that there are still significant differences between the present solution and that of Lyne (1971).

We now discuss the effect of above flow structure on the time development of the bottom. Two contributions to $\tilde{\mathscr{A}}_r$ can be identified. The first is associated with the steady component of the fluid velocity evaluated at $y^* = \frac{1}{2}d^*$ and reads

$$\tilde{\mathscr{A}}_{r1} = \mathrm{Re}\left\{-\frac{1}{2\pi}\int_0^{2\pi} i\alpha\, Qb2 \left|2\frac{\partial \psi_0}{\partial y}\right|^{b-1}\left[\frac{\partial^2 \psi_0}{\partial y^2} + \frac{\partial \Phi_1}{\partial y}\right] dt\right\}. \tag{37}$$

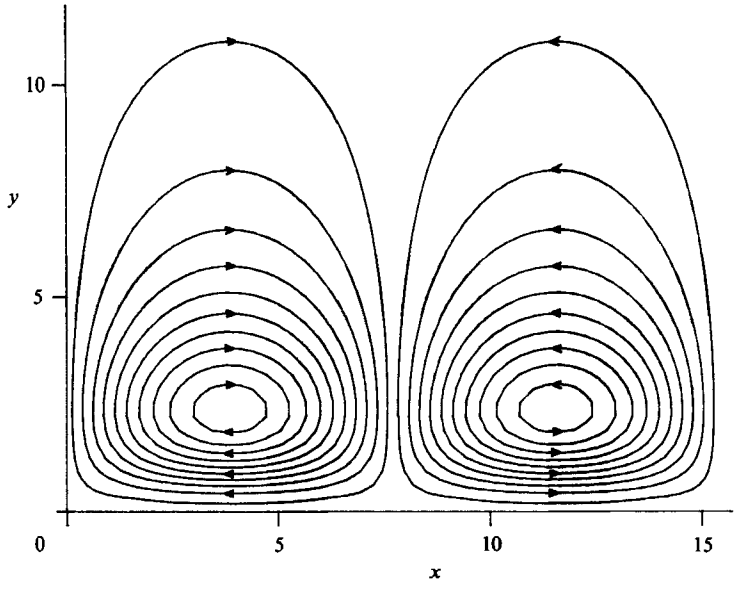

FIGURE 1. Steady streaming at order ϵ of the viscous oscillatory flow over a wavy wall ($\alpha = 0.4, R_\delta = 0.1$).

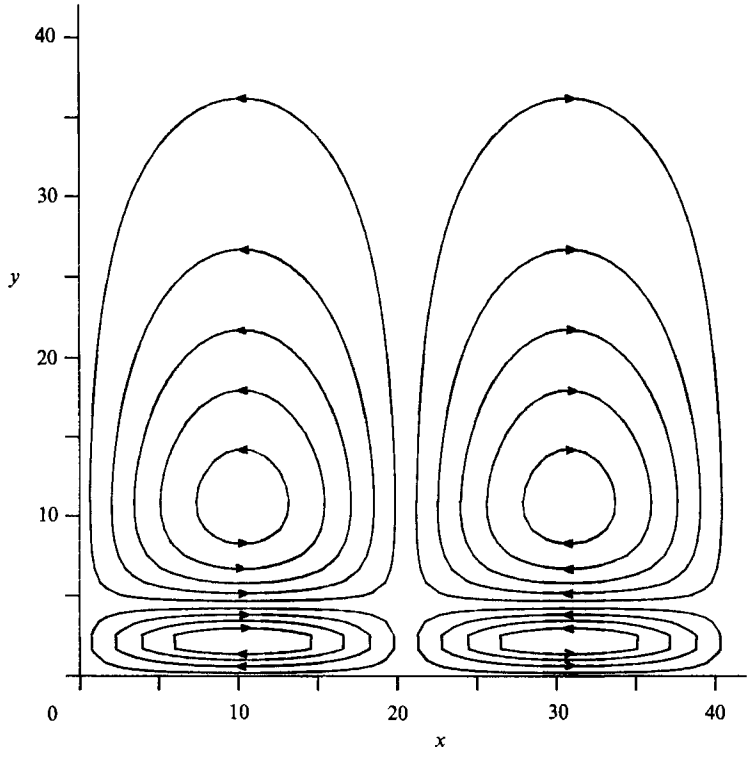

FIGURE 2. Steady streaming at order ϵ of the viscous oscillatory flow over a wavy wall ($\alpha = 0.15, R_\delta = 0.1$).

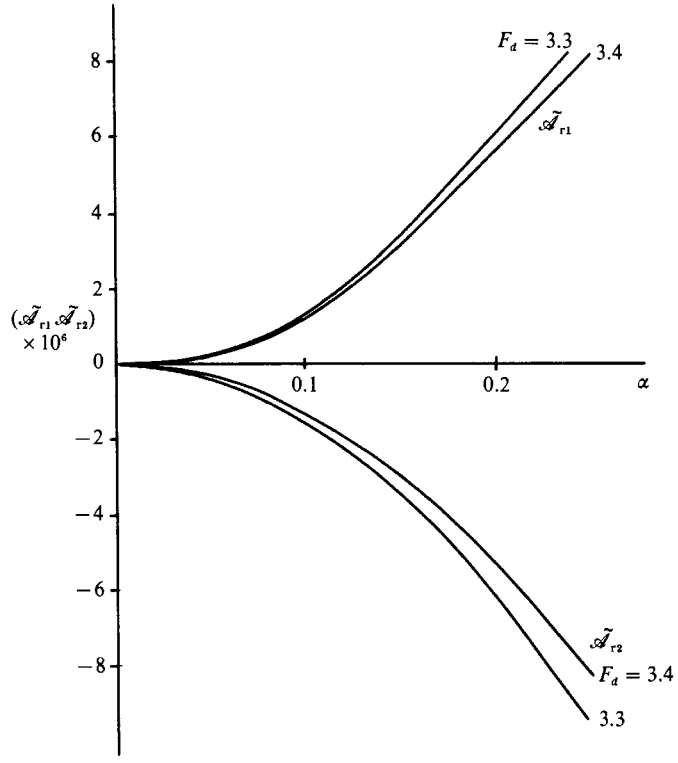

FIGURE 3. Stabilizing ($\tilde{\mathscr{A}}_{r1}$) and destabilizing ($\tilde{\mathscr{A}}_{r2}$) real parts of the average growth coefficient ($\tilde{\mathscr{A}}_r$) of the bottom perturbation versus the wavenumber α ($R_\delta = 80$, $R_d = 100$, $s = 2.65$, $\beta = 0.15$).

If d^* is much smaller than δ^* this contribution is destabilizing since the steady drift close to the bed tends to carry sediment from the troughs to the crests of the perturbation, thus causing its growth. Sleath (1984) suggested that for larger values of d^* a different behaviour may occur. Indeed, as previously described, depending on the values of α and R_δ a region not far from the bed may be present where the steady drift is directed from the crests to the troughs of the perturbation.

The second contribution is due to the component of gravity along the tangent to the bed profile which has a stabilizing effect. We find

$$\tilde{\mathscr{A}}_{r2} = \mathrm{Re}\left\{\frac{1}{2\pi}\int_0^{2\pi} \mathrm{i}\alpha Qb2\left|2\frac{\partial\psi_0}{\partial y}\right|^{b-1}\left[\frac{\mathrm{i}\alpha\beta R_d}{2F_d^2}\right]\mathrm{d}t\right\}. \tag{38}$$

Indeed gravity opposes the tendency of the flow to carry sediment from the troughs to the crests of the perturbation, thus causing decay of the latter.

The behaviour of a perturbation for given values of $\alpha, R_\delta, R_d, F_d$ is thus controlled by a balance between the two effects described above. In figure 3 the two contributions are plotted versus α for fixed typical values of F_d, R_d, R_δ. It appears that the stabilizing effect due to gravity grows very rapidly as α increases, for large α reaching absolute values which exceed the destabilizing contribution due to the flow. However, a range of α may exist where destabilizing effects prevail over stabilizing effects. Similar behaviour was found for different values of F_d, R_d, R_δ.

In figure 4 the value of $\tilde{\mathscr{A}}_r$, obtained by adding the above two contributions, is plotted versus α for fixed values of R_δ and R_d and different values of F_d. It appears

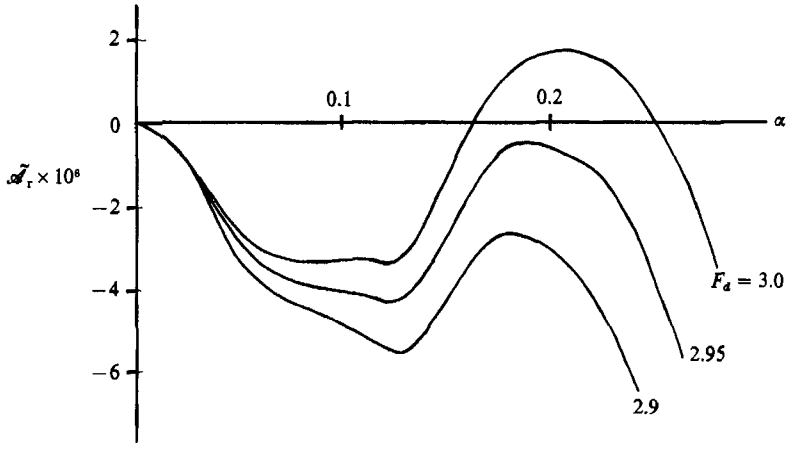

FIGURE 4. Real part of average growth coefficient $\mathscr{A}_r$ of the bottom perturbation versus the wavenumber α ($R_\delta = 80$, $R_d = 80$, $s = 2.65$, $\beta = 0.15$).

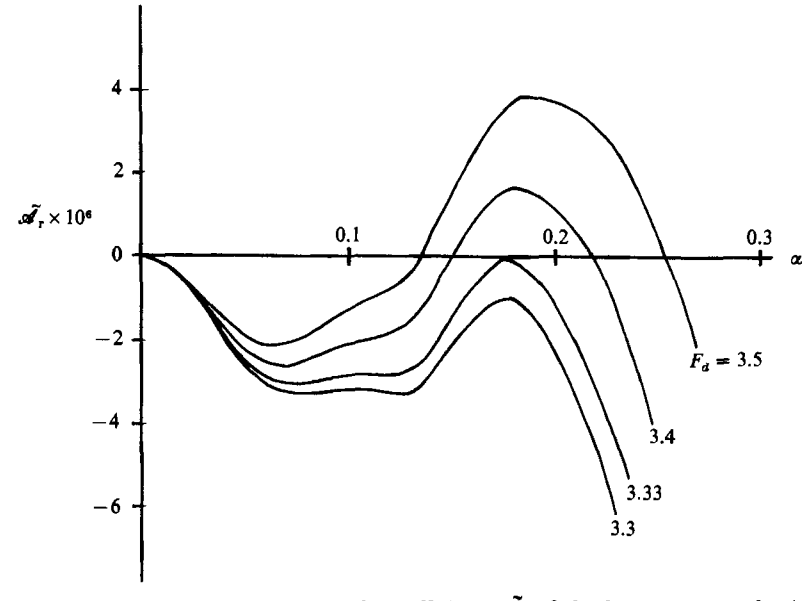

FIGURE 5. Real part of average growth coefficient $\mathscr{A}_r$ of the bottom perturbation versus the wavenumber α ($R_\delta = 80$, $R_d = 100$, $s = 2.65$, $\beta = 0.15$).

that a critical value of F_d exists such that: for F_d less than F_{dc} bottom perturbations decay for each value of the wavenumber α; for F_d larger than F_{dc} bottom perturbations, characterized by values of α falling within a restricted range, experience an average amplification within a cycle.

Different values of the sediment Reynolds number (see figure 5) do not change the qualitative behaviour of the results. However, an increase of R_d causes a decrease of the critical wavenumber α_c. This fact implies that, for given characteristics of the wave, sediments with larger grain size are expected to form longer ripples. This trend is indeed experimentally observed. In table 1 experimental results from Sleath (1976) are reported. Pairs of runs are chosen such that all the parameters are similar except

$d^* = 0.404$ mm			$d^* = 1.14$ mm		
T^* (s)	U_0^* (cm/s)	l^* (cm)	T^* (s)	U_0^* (cm/s)	l^* (cm)
1.77	35.5	6.00	1.80	34.9	9.33
1.83	51.5	8.66	1.87	50.4	11.8
1.84	51.2	8.00	—	—	—
2.54	37.1	6.24	2.68	35.2	12.0
2.64	35.7	6.45	—	—	—
2.80	33.7	5.95	2.72	34.6	12.75
1.75	71.8	10.23	1.83	65.23	16.75
1.97	63.8	8.65	1.97	60.6	16.00
2.65	47.4	8.26	2.62	45.6	11.17
3.2	39.3	6.14	3.19	37.4	12.83

TABLE 1. Experimental results for Sleath (1976): $\nu \approx 10^{-2}$ cm^2/s, $\rho_s/\rho = 2.65$

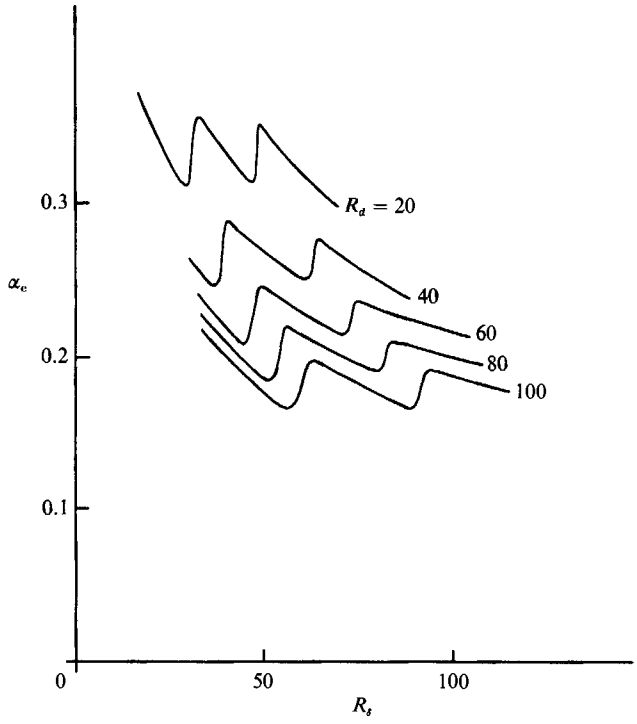

FIGURE 6. Critical wavenumber α_c versus the Reynolds number of the flow for the different values of the sediment Reynolds number ($s = 2.65$, $\beta = 0.15$).

for the grain size. It appears that the coarser sand produces ripples the wavelength of which can be twice as long as that found for the finer sand. Of course this trend is limited by the requirement that d^* shall not be much larger than δ^* for the theory to be valid. Indeed if $d^* \gg \delta^*$ Stokes flow becomes not significant. This theoretical result is also clearly detectable in figure 6 where the critical wavenumber α_c is plotted versus the Stokes Reynolds number for different values of the sediment Reynolds number. The strong variability of α_c as function of R_δ for fixed R_d is related to the value of the ratio between the amplitude of sediment displacement s^* and ripple

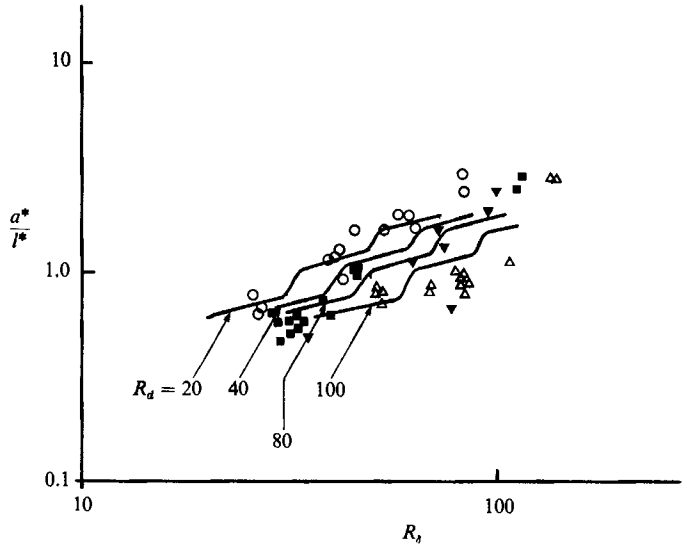

FIGURE 7. Ratio between fluid displacement a^* and the critical ripple wavelength l^* versus the Reynolds number of the flow for different values of the sediment Reynolds number ($\beta = 0.15$) (experimental data by Blondeaux *et al.* 1988). ○, $5 < R_d < 15$; ■, $15 < R_d < 25$; ▼, $25 < R_d < 35$; △, $50 < R_d < 80$.

wavelength l^*. Indeed during a wave period, sediments are subject to the action of a different number of steady recirculating cells depending on the value of s^*/l^*. When the number of steady recirculating cells which affect the motion of sediment grains changes, a strong variation of α_c is produced. Indeed s^*/l^* is related to the value of r (r is the ratio between fluid displacement far from the bottom and ripple wavelength) and it is easy to verify that the maxima and the minima of α_c lie on curves along which r is constant (r is equal to $\alpha R_\delta/4\pi$).

A comparison between the present theoretical findings and experimental data by Blondeaux *et al.* (1988) is shown in figure 7 where the ratio between the amplitude of fluid displacement a^* and the critical ripple wavelength l^* is plotted versus R_δ. The theoretical predictions are shown for four different values of R_d (20, 40, 80, 100) and the experimental data are characterized by values of R_d falling in the ranges (5, 15), (15, 25), (25, 35), (50, 80). The agreement seems satisfactory even though the theory somewhat underpredicts the wavelength of the ripples that appear.

From the above results it is possible to obtain marginal stability curves. An example is shown in figure 8 where the values of F_d such that $\tilde{\mathscr{A}}_r$ vanishes are plotted versus α for particular values of R_d and R_δ. As previously discussed, for fixed values of the sediment and flow Reynolds numbers a critical value of the particle Froude number can be easily determined below which a flat bottom configuration is stable. The critical value of the Froude number can then be plotted versus the Stokes Reynolds number R_δ for different values of R_d. The plane (F_d, R_δ) is thus divided into two regions (see figure 9): in the lower region the bed is expected to remain flat while in the upper region ripples are expected to appear. A comparison of the theory with experimental data by Blondeaux *et al.* (1988) is shown in figure 10. A good agreement is found except for R_δ less than R_d. Indeed in this situation d^* is greater than δ^* and the theory cannot be applied because Stokes flow is no longer significant.

Finally, some further comparisons between the present theory and experimental

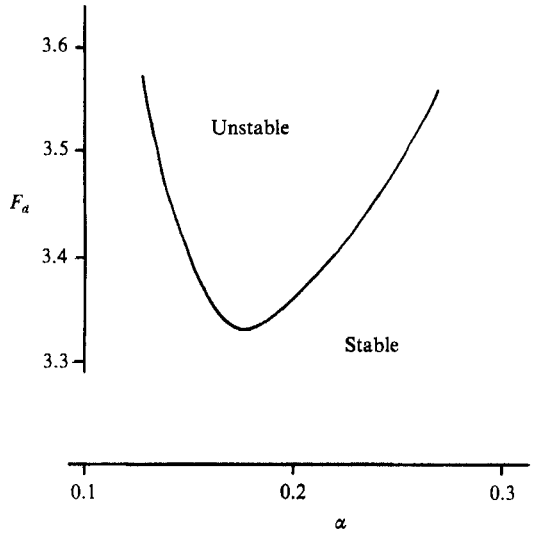

FIGURE 8. Marginal stability curve in the (F_d, α)-plane for $R_\delta = 80$ and $R_d = 100$ ($s = 2.65$, $\beta = 0.15$).

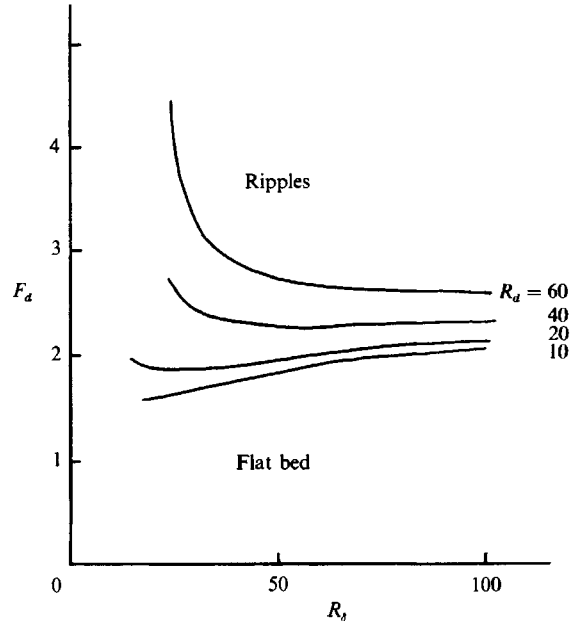

FIGURE 9. Limiting curves between flat bed and rippled bed regimes in the (R_δ, F_d)-plane for different values of R_d ($s = 2.65$, $\beta = 0.15$).

data are pursued in figure 11 where the experimental and theoretical values of the ratio between the amplitude of fluid oscillations and the ripple wavelength are plotted versus the parameter $[\rho d^*/(\rho_s - \rho) g T^{*2}]$ which has been proposed by many authors as that controlling ripple wavelength. It is worth pointing out that experimental data appearing in figure 11 are such that the ratio between ripple height and length is less than 0.1 and, following Sleath (1984), flow separation can

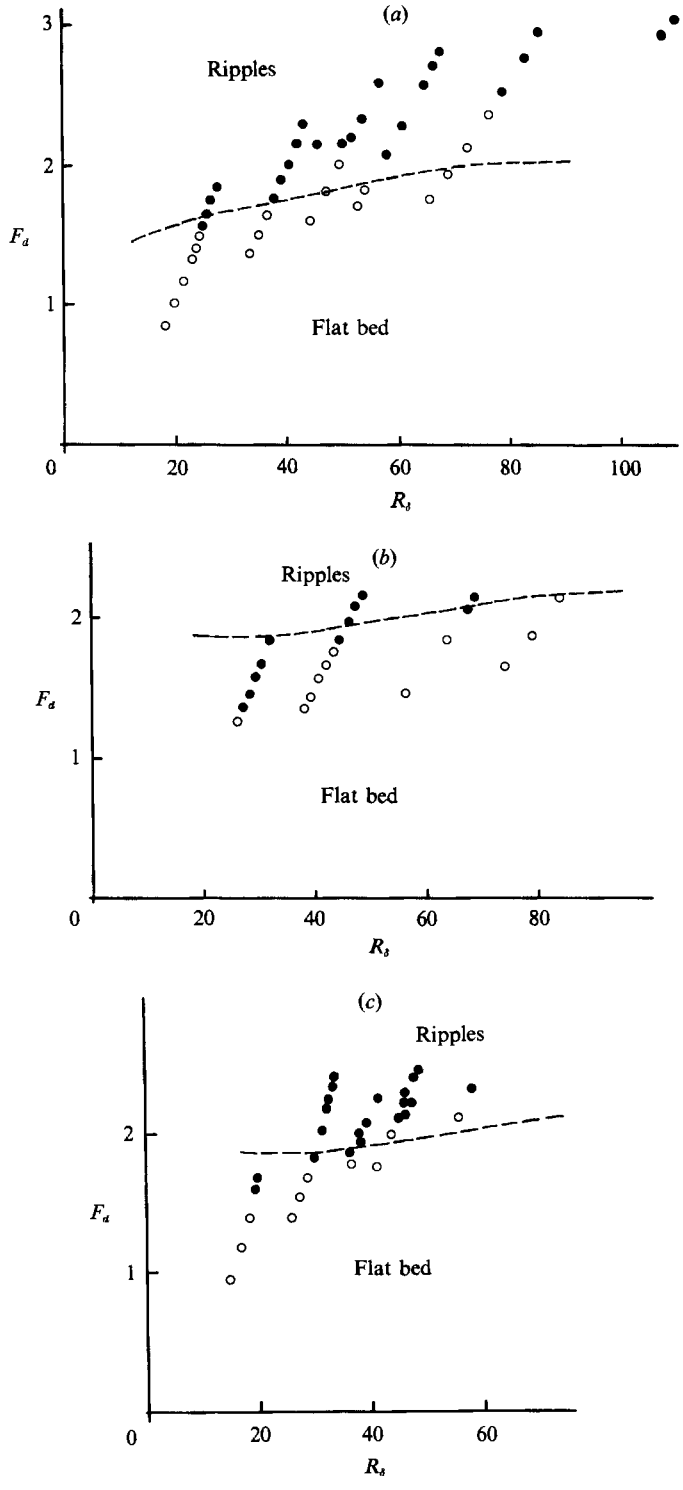

FIGURE 10. Comparison between theory and experimental data from Blondeaux *et al.* (1988) of limiting curves between flat bed and rippled bed regimes in the (R_s, F_d)-plane ($\beta = 0.15$), (*a*) $R_d = 10$, $s = 2.65$, (*b*) $R_d = 20$, $s = 2.65$, (*c*) $R_d = 20$, $s = 1.15$. Experimental data are such that R_d ranges between (*a*) 5, 15, (*b*) 14, 24, (*c*) 15, 25 (●, rippled bed; ○, flat bed).

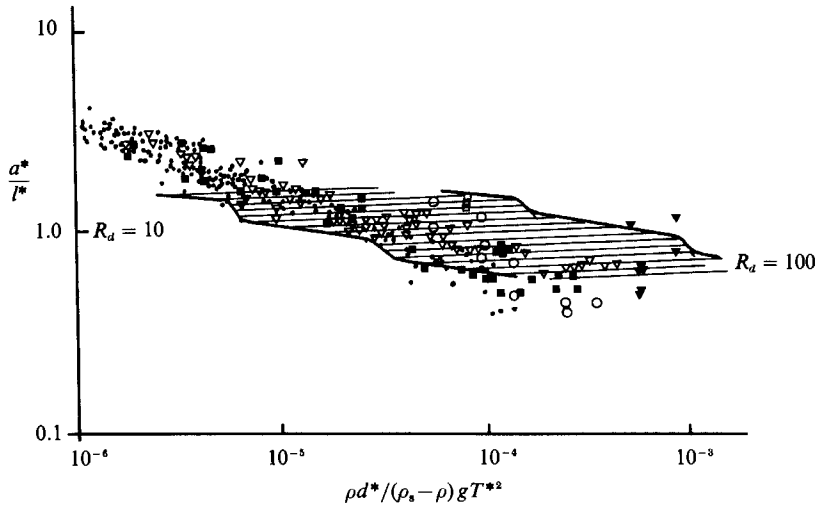

FIGURE 11. Ratio between fluid displacement a^* and predicted critical ripple wavelength l^* plotted versus the parameter $\rho d^*/(\rho_s-\rho)gT^{*2}$. ●, Manohar (1955); ▼, Kennedy & Falcon (1965); □, Yalin & Russel (1962); ○, Horikawa & Watanabe (1967); ▽, Sleath (1976); ■, Blondeaux *et al.* (1988).

be assumed absent. It can be concluded that all data refer to rolling-grain ripples. In figure 11 the theoretical predictions fall within a dashed region delimited by two curves which correspond to two different values of R_d, namely 10 and 100. The relatively large scatter in the experimental data appears to suggest the impossibility of predicting ripple wavelength on the basis of only one parameter. In figure 11 theoretical predictions for very low values of $\rho d^*/(\rho_s-\rho)gT^{*2}$ are not shown because such values of this parameter imply a turbulent flow. The satisfactory agreement between the present theoretical predictions and experimental observations in spite of a still fairly rough modelling of sediment transport appears to support the following main conclusions of this work:

(i) ripple formation is essentially an instability process;

(ii) the destabilizing effect is due to steady streaming associated with secondary flow which under certain conditions tends to carry sediment from the troughs to the crests of the perturbation. The stabilizing effect is gravity acting on sediment particle.

Of course we cannot predict, on the basis of a linear analysis, whether growing perturbations eventually reach a finite equilibrium amplitude. This aim is pursued in the companion paper (Vittori & Blondeaux 1990) where the weakly nonlinear development of the most unstable bottom perturbation predicted by the present linear theory for values of the parameters close to the critical conditions is followed. Results described in Vittori & Blondeaux (1990) will allow us to determine the geometrical shape of finite-amplitude rolling-grain ripples and the conditions for rolling-grain ripples to evolve into vortex ripples.

This work was supported by the Italian Ministry of Education under contract MPI 60%. Many thanks are due to Dr G. Vittori for discussions on various issues arising from the work.

REFERENCES

BAGNOLD, R. A. 1946 Motion of waves in shallow water. Interaction of waves and sand bottoms. *Proc. R. Soc. Lond.* A **187**, 1–15.

BLONDEAUX, P. 1987 Turbulent boundary layer at the bottom of gravity waves. *J. Hydraul. Res.* **25**, 447–464.

BLONDEAUX, P. & SEMINARA, G. 1979 Transizione incipiente al fondo di un'onda di gravità. *Rendiconti Accad. Naz. Lincei* **67**, 407–417.

BLONDEAUX, P., SLEATH, J. F. A. & VITTORI, G. 1988 Experimental data on sand ripples in an oscillatory flow. *Rep.* 01/88. Inst. Hydraulics, University of Genoa.

ENGELUND, F. 1974 Flow and bed topography in channel bends. *J. Hydraul. Div. ASCE* **100** (HY 11), 1631–1648.

FREDSØE, J. 1974 On the development of dunes on erodible channels. *J. Fluid Mech.* **64**, 1–16.

GRASS, J. A. & AYOUB, N. M. 1982 Bed load transport of time sand by laminar and turbulent flow. In *Proc. 18th Coastal Engineering Conference* (ed. B. L. Edge), pp. 1589–1599.

HORIKAWA, K. & WATANABE, A. 1967 A study of sand movement due to wave action. *Coastal Engng Japan* **10**, 39–57.

HINO, M., SAWAMOTO, M. & TAKASU, S. 1976 Experiments on transition to turbulence in an oscillatory pipe flow. *J. Fluid Mech.* **75**, 193–207.

KANEKO, A. 1981 Oscillation sand ripples in viscous fluids. *Proc. Japan. Soc. Civil Engrs* **307**, 113–124.

KANEKO, A. & HONJI, H. 1979 Double structures of steady streaming in the oscillatory viscous flow over a wavy wall. *J. Fluid Mech.* **93**, 727–736.

KENNEDY, J. F. & FALCON, M. 1965 Wave-generated sediment ripples. *MIT Hydrodyn. Lab. Rep.* 86.

LI, H. 1954 Stability of oscillatory laminar flow along a wall. *US Army, Beach Erosion Board, Tech. Memo* 47.

LOFQUIST, K. E. B. 1978 Sand ripples growth in an oscillatory-flow water tunnel. *US Army Corps of Engng Coastal Engng Res. Center Tech. Paper* 78-5.

LYNE, W. H. 1971 Unsteady viscous flow over wavy wall. *J. Fluid Mech.* **50**, 33–48.

MANOHAR, M. 1955 Mechanics of bottom sediment movement due to wave action. *US Army, Beach Erosion Board Tech. Memo* 75.

MERKLY, P. & THOMANN, H. 1975 Transition to turbulence in oscillatory pipe flow. *J. Fluid Mech.* **68**, 567–575.

SEMINARA, G. & HALL, P. 1976 The centrifugal instability of a Stokes layer theory. *Proc. R. Soc. Lond.* A **350**, 299–316.

SERGEEV, S. I. 1966 Fluid oscillations in pipes at moderate Reynolds number. *Fluid Dyn.* **1**, 21–22.

SLEATH, J. F. A. 1976 On rolling-grain ripples. *J. Hydraul. Res.* **14**, 69–81.

SLEATH, J. F. A. 1978 Measurements of bed load in oscillatory flow. *J. Waterway Port Coastal Ocean Engng Div.*, ASCE **104** (WW3), 291–307.

SLEATH, J. F. A. 1984 *Sea Bed Mechanics.* Wiley.

STOKES, A. G. 1851 On the effect of the internal friction of fluids on the motion of pendulums. *Trans. Camb. Phil. Soc.* **9**, 20–21.

TROMANS, P. 1976 The stability of oscillating pipe flow. Abstract of lecture given at *Euromech 73: Oscillatory Flows in Ducts, Aix-en-Provence, April 13–15.*

UDA, T. & HINO, M. 1975 A solution of oscillatory viscous flow over a wavy wall. *Proc. Japan. Soc. Civil Engrs* **237**, 27–36.

VITTORI, G. 1988 Non-linear viscous oscillatory flow over a small amplitude wavy wall. *J. Hydraul. Res.* **27**, 267–280.

VITTORI, G. & BLONDEAUX, P. 1990 Sand ripples under sea waves. Part 2. Finite-amplitude development. *J. Fluid Mech.* **218**, 19–39.

YALIN, M. S. & RUSSEL, R. C. H. 1962 Similarity in sediment transport due to waves. *Proc. 8th Conf. Coastal Engng Mexico* (ed. J. W. Johnson), pp. 151–167.